Monitoring surface water area variations of reservoirs using daily MODIS images by exploring sub-pixel information

Feng Ling[a], Xinyan Li[a,b], Giles M. Foody[c], Doreen Boyd[c], Yong Ge[d], Xiaodong Li[a], Yun Du[a]

[a] *Key Laboratory for Environment and Disaster Monitoring and Evaluation, Hubei, Innovation Academy for Precision Measurement Science and Technology, Chinese Academy of Sciences, Wuhan 430077, China*

[b] *The University of Chinese Academy of Sciences, Beijing 100864, China*

[c] *School of Geography, University of Nottingham, University Park, Nottingham NG7 2RD, U.K.*

[d] *State Key Laboratory of Resources and Environmental Information System, Institute of Geographic Sciences & Natural Resources Research, Chinese Academy of Sciences, Beijing 100101, China*

Abstract:

Information on the temporal variation of surface water area of reservoirs is fundamental for water resource management and is often monitored by satellite remote sensing. Moderate Resolution Imaging Spectroradiometer (MODIS) imagery is an attractive data source for the routine monitoring of reservoirs, however, the accuracy is often limited due to the negative impacts associated with its coarse spatial resolution and the effects of cloud contamination. Methods have been proposed to solve these two problems independently but it remains challenging to address both problems simultaneously. To overcome this, this paper proposes a new approach that aims to monitor reservoir surface water area variations accurately and timely from daily MODIS images by exploring sub-pixel scale information. The proposed approach used estimates of reservoir water areas obtained from cloud-free and relatively fine spatial resolution Landsat images and water fraction images by spectral unmixing of coarse MODIS imagery as reference data. For each MODIS pixel, these reference reservoir water areas and their corresponding pixel water fractions were used to construct a linear regression equation, which in turn may be applied to predict the time series of reservoir water areas from daily MODIS water fraction images. The proposed approach was assessed with 21 reservoirs, where the correlation coefficients between reservoir water areas predicted by the common pixel-based analysis method and altimetry water levels were all less than 0.5. With the proposed sub-pixel analysis method, the resultant correlation coefficients were much improved, with eleven values larger than 0.5 including six values larger than 0.8 and the highest value of 0.94. The results show that the proposed sub-pixel analysis method is superior to the pixel based analysis method. The proposed method makes it possible to directly estimate the whole reservoir water area from,

potentially, an individual cloud-free MODIS pixel, and is a promising way to improve the accuracy in the usability of MODIS images for the monitoring of reservoir surface water area variations.

Keywords: MODIS, sub-pixel analysis, surface water, reservoir area

1. Introduction

Reservoirs are valuable freshwater resources that play an important role in topics such as water supply, irrigated agriculture, hydropower generation and navigation. Monitoring the spatial and temporal variations of reservoir water storage is critical in water management and in the understanding of the impact of human activities and climate change on the hydrological system (Downing et al. 2006; Gao 2015; Lehner et al. 2011; Pekel et al. 2016; Zhou et al. 2016). Important information about reservoirs, including water level and water area, can be provided by *in-situ* monitoring networks, however, a large number of reservoirs in the world are still lacking these data, especially those in developing countries. In the past decades, satellite data have widely been used to monitor reservoirs globally (Alsdorf et al. 2007; Busker et al. 2019; Cretaux et al. 2016; Doernhoefer and Oppelt 2016; Duan and Bastiaanssen 2013; Tong et al. 2016). Two fundamental variables can be acquired routinely from satellite data: water height can be monitored by satellite altimetry (Birkett and Beckley 2010; Schwatke et al. 2015; Zhang et al. 2011), and surface water area can be estimated from conventional remotely sensed imagery (Gao et al. 2012; Huang et al. 2018; Khandelwal et al. 2017; Sheng et al. 2016; Verpoorter et al. 2014; Yao et al. 2019).

Presently, a variety of remotely sensed image sources are available for surface water mapping (Alsdorf et al. 2007; Huang et al. 2018; Pekel et al. 2016; Seaton et al. 2020; Tulbure and Broich 2013). One of the most popular sources of remotely sensed imagery for reservoir monitoring is the series of sensors that have been carried by the Landsat satellites (Arvor et al. 2018; Avisse et al. 2017; Duan and Bastiaanssen 2013; Ma et al. 2019; Sheng et al. 2016; Yao et al. 2019; Zhang et al. 2017; Zhao and Gao 2018). The Landsat sensor imagery have a spatial

resolution of 30 m and are available globally for over 40 years, making them a valuable resource for relatively long-term and high spatial resolution monitoring of water area dynamics. However, its relatively coarse temporal resolution, arising mainly from its ~16-day re-visit period, together with the effect of cloud contamination, limits the frequency with which suitable data are acquired for reservoir monitoring. Another popular source of remotely sensed imagery is the Moderate Resolution Imaging Spectroradiometer (MODIS) (Chen et al. 2014; Gao et al. 2012; Khandelwal et al. 2017; Ma et al. 2019; Zhang et al. 2014). MODIS offers the ability to acquire images on a daily basis which is very attractive for routine reservoir monitoring at regional to global scales. However, the accuracy of reservoir surface water areas monitored by the MODIS images is often limited by two main problems: the coarse spatial resolution and the cloud contamination.

MODIS images have a coarse spatial resolution, with the finest imagery available at about 250 m. It is well known that the ability to estimate and monitor reservoir surface water area depends on the relationship between the pixel size of the remotely sensed images and the extent of area variation (Busker et al. 2019; Khandelwal et al. 2017). In general, to estimate the surface water area of a reservoir, a water body mapping algorithm (Feyisa et al. 2014; Frazier and Page 2000; McFeeters 1996; Xu 2006) should be applied to the images to generate corresponding surface water maps. The mapping of reservoir surface water area is often undertaken at the the pixel scale, meaning that a pixel in the remotely sensed images should represent an area that is either completely covered by water or by land. When coarse spatial resolution images are used, the pixels located near the boundaries between water and land often cannot be mapped accurately as they are of mixed composition with the land water boundary running within their

area. Consequently, the reservoir water surface area may be substantially mis-estimated from coarse resolution imagery (Ling et al. 2019; Park et al. 2019).

Another challenge in the monitoring of reservoir surface water area with the MODIS images is the effect of cloud contamination (Khandelwal et al. 2017; Klein et al. 2017; Yao et al. 2019; Zhao and Gao 2018). When the target reservoir is fully or partly covered by clouds (or cloud shadows), its surface water area is difficult to estimate accurately because it is impossible to determine whether the cloud contaminated pixels are of water or land directly. Selecting cloud-free images can overcome this problem, however, this is at the cost of reducing the temporal density of imagery and so the ability to monitor at a high temporal frequency.

Methods have been proposed to solve these two problems individually. For the coarse spatial resolution problem, a promising method to aid accurate estimation of the water area is based on spectral unmixing which enables analysis at a sub-pixel scale (Li et al. 2019a; Li et al. 2013a; Li et al. 2016; Ma et al. 2014; Muad and Foody 2012). Different to conventional pixel based approaches, spectral unmixing does not assign a coarse spatial resolution pixel a 'hard' (single class) label but instead decomposes the observed spectral signature to indicate the fractional coverage of each class estimated to lie within the area represented by the pixel (Foody and Cox 1994; Keshava and Mustard 2002). Thus, spectral unmixing allows more accurate estimation of surface water area from coarse resolution imagery (Park et al. 2019).

For the cloud contamination problem, several cloud-filtering algorithms have been proposed to predict class labels (water or land) of cloudy pixels using the information provided by other cloud-free image pixels (Khandelwal et al. 2017; Li et al. 2019b; Yao et al. 2019). As a result, the whole reservoir surface water area can be calculated from partly cloudy images,

and the frequency of reservoir monitoring increased.

In practice, however, reservoir monitoring is challenging as the problems associated with both coarse spatial resolution and cloud contamination ideally need to be considered simultaneously. On one hand, the spectral unmixing analysis can only be applied to cloud-free pixels, and the presence of cloud will degrade the analysis since a cloud covered pixel will convey little or no information on ground cover. On the other hand, cloud-filtering algorithms can only be used to estimate information about cloudy pixels at the pixel scale. If fine spatial resolution images, such as from Landsat sensor images, are used, the surface water area estimated can be highly accuracy (Yao et al. 2019; Zhao and Gao 2018), but only at a low temporal frequency. While MODIS offers the potential for monitoring at a fine temporal resolution, its coarse spatial resolution limits the ability to estimate water area accurately with the utility of cloud-filtering algorithms. A means to address both of these problems is required if the full potential of MODIS for monitoring surface water area is to be fulfilled.

A key limitation of existing cloud-filtering algorithms is that they require a water map, with which the reservoir surface water area can then be counted. This processing procedure is intuitive, however, we argue that recovering the land cover information of those cloudy pixels is an unnecessary step, while estimating the reservoir surface water area directly from the cloud-free pixels that are present is a more effective way. The latter is similar to the methods used for river discharge estimation with the MODIS images, in which the river discharge is estimated with the relationship between the river discharge and the water coverage of MODIS pixels located in the river (Tarpanelli et al. 2017; Tarpanelli et al. 2013; Van Dijk et al. 2016).
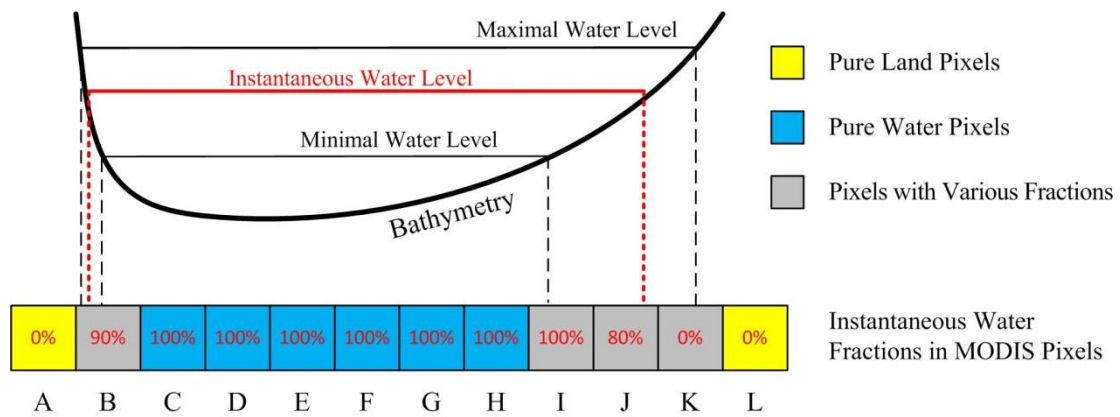
Fig. 1. A diagram showing a hypothetical cross-section of a reservoir and water fractions in corresponding MODIS pixels at the instantaneous water level shown as red. Pixels A and L are located outside of the extent with the maximal water level and are always representing areas of pure coverage by land. Pixels C to H are located inside the extent of the reservoir even at its minimal water level and hence always represent an area of pure coverage by water. At all water levels pixel B is of mixed composition. Pixels I,J and K may be pure or mixed depending on the water level (e.g. pixel I is mixed when the water is at its minimal level but pure water at the instantaneous water level; while pixel J is pure land when the water is at its minimal level but mixed at the instantaneous water level). Note that fluctuation in the area extent of the reservoir is least where the terrain boundary at the reservoir is sharp and greatest where the boundary is gradual; the former is harder to detect than the latter as the changes in extent are all sub-pixel.

The extent of a reservoir will fluctuate with the height of the water level (Fig. 1). In general, the water extent increases with the increase of water level, and the magnitude of water area variation is associated with the bathymetry. The water extent reaches the largest when the water level is at the maximal, and the water extent is the smallest when the water level is at the minimal. The water coverage within MODIS pixels at different locations along the cross-section shows different change trend with the water level fluctuation. Some pixels have constant

8

water percentages that are not related with the water level. For example, the pixels located outside of the largest extent, including A and L (Fig. 1), are always representing complete coverage land, while the pixels located inside the smallest extent, including C to H, are always full of water. In contrast, for the MODIS pixels lying within the zone covered by the reservoir at its minimal and maximal water levels, (i.e. pixels B, I, J and K), the extent of water coverage will change with the water level. The reservoir has a relatively steep slope in the left side, and the water extent variation is relatively small and is limited to the pixel B. When a conventional pixel-based scale of analysis is used to estimate the water area in such a pixel it would always be as water at any water level because its water coverage is always is larger than 0.5 (i.e. >50% of pixel B's area is covered in water). However, the sub-pixel scale variations in surface water extent in the pixel could be assessed if a sub-pixel analysis was undertaken. Moreover, the variation in water coverage in pixel B is correlated with the water level change, and the latter could be inferred from the former if a predictive relationship between water coverage and height can be established. Similarly, the water coverage in pixels I to K is also related with the whole reservoir water area, although the relationship will be different according to the spatial location and bathymetry within pixels. Critically, however, if any cloud-free pixel that has a strong relationship between its water fraction area and the reservoir surface water area, such as pixel B (Fig. 1), then this individual pixel may be used to estimate the areal extent of the entire reservoir even if all other pixels are cloud contaminated.

In this paper, we propose a novel method that aims to estimate the temporal variation of reservoir surface water areas from MODIS images. The overall objectives are: (i) to increase the accuracy of reservoir surface water monitoring using MODIS images, and (ii) to address

the coarse spatial resolution problem and the cloud contamination problem, simultaneously.

2. Data

The proposed method estimates reservoir surface water area with the use of fraction images from MODIS images combined with a predictive regression to link the fraction to whole reservoir water coverage, with the regression equation based on reference data from relative fine resolution Landsat images. The main input data sources of the proposed method are MODIS and Landsat images.

2.1 Study reservoirs

A set of reservoirs were selected for the analyses from the result reported by Khandelwal et al. (2017). In their method, an initial map including water, land, and missing labels was first produced from MODIS images by supervised classification. Post-processing was then used to enhance the imperfect pixel labels, using an elevation based label correction algorithm. Finally, the map including only water and land labels was produced and used to estimate reservoir water area. Their method was tested in 94 reservoirs and it was found that the predicted reservoir water areas showed higher correlation with the altimetry water levels, compared to previous studies. However, it was also noticed that there were 22 reservoirs for which the correlation coefficient between water area and water level was less than 0.5. The poor results for these 22 reservoirs was caused mainly by their relatively small dynamic region widths, which are about the size of several MODIS pixels. Standard pixel-based method cannot accurately capture such small surface water area variations. These 22 reservoirs were selected for analysis as they represent cases which may benefit from sub-pixel scale assessment. One reservoir, however,

10

had to be excluded as suitable altimetry data on water level were unavailable. The 21 reservoirs

used to test the ability of the sub-pixel scale based method proposed in this study are shown in

Figure 2 and the results can be compared to estimates obtained by the standard pixel-based
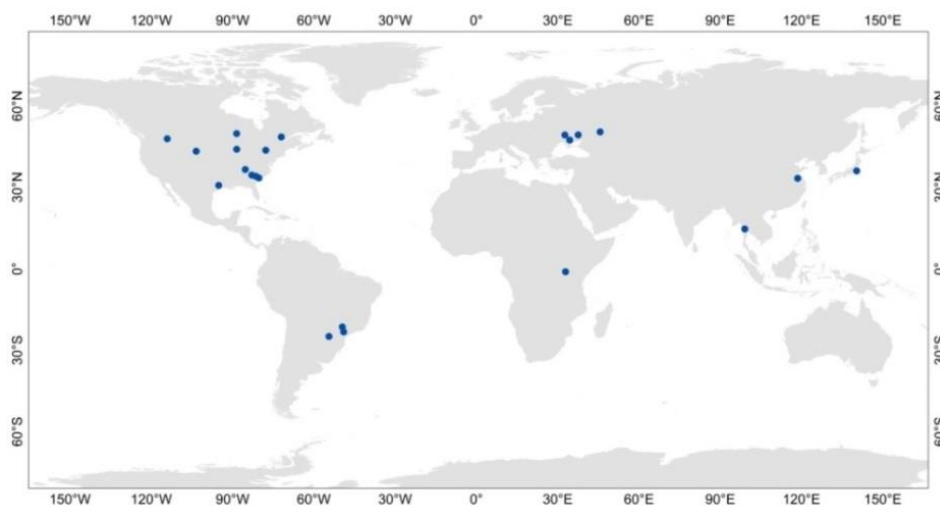
method.

Fig. 2. Locations of the study reservoirs.

2.2 MODIS imagery

The MODIS images used were the MCD43A4 Version 6 Nadir Bidirectional Reflectance

Distribution Function (BRDF) Adjusted Reflectance (NBAR) dataset. Compared to the

previous MCD43A4 Version 5 product, which is updated every 8-days, the new MCD43A4

Version 6 dataset is produced daily at 500 m resolution (Wang et al. 2018). The improvement

of temporal resolution of the dataset makes daily reservoir monitoring possible. In this study,

the NBAR layer of MODIS band 2 that has a strong spectral contrast between water and land

(Tarpanelli et al. 2013) was used. The quality layer of this band provided in the MCD43A4

product includes three quality flags: 0 means this pixel was processed with full BRDF

inversions, 1 means this pixel was processed but with magnitude BRDF inversions, and 255

11

means a void reflectance value. The pixels processed with full or magnitude BRDF inversions were considered to be valid and used in the analysis.

2.3 Landsat imagery

The Landsat images used were the orthorectified top-of-atmosphere reflectance data from Landsat 5 Thematic Mapper (TM), and Landsat 8 Operational Land Imager (OLI) sensors, both with a 30 m spatial resolution and a revisit interval of 16 days. Landsat images were used to provide reference data on reservoir surface water areas for the period of 2000 to 2018. To ensure the estimated reservoir surface water areas have a relative high accuracy, only cloud-free Landsat images were used. The *SimpleCloudScore* algorithm in the Google Earth Engine was applied to detect clouds in Landsat images (Gorelick et al. 2017; Wayand et al. 2018; Yao et al. 2019).

2.4 Radar Altimetry

Radar altimetry water levels in the Global Reservoir and Lake Monitoring (GREALM) dataset (Birkett 1995; Birkett and Beckley 2010) were used to assess the proposed method (Khandelwal et al. 2017). The dataset includes two types of time series of water levels. One is GREALM-10, which merges Topex/Poseidon, Jason-1, and Jason-2 relative water level variation at 10-day intervals. The other is GREALM-35, which is the ENVISAT relative water level variation at 35-day intervals. For each reservoir, the water level time series that had the higher correlation coefficient with the reservoir surface water area time series estimated by the pixel based MODIS analysis method reported by Khandelwal et al. (2017) was selected for the assessment.

3. Methodology

To estimate the time series of reservoir surface water areas from daily MODIS images, the proposed method has four main processing steps: (1) Calculate reference reservoir surface water areas from cloud-free Landsat images; (2) Extract water fraction images from MODIS images; (3) Regress water fraction values and reference reservoir surface water areas for each MODIS pixel; (4) Predict the time series of reservoir surface water areas from daily water fraction images using the regression equations. Figure 3 shows the flowchart of the proposed method, and each is discussed in the following subsections.
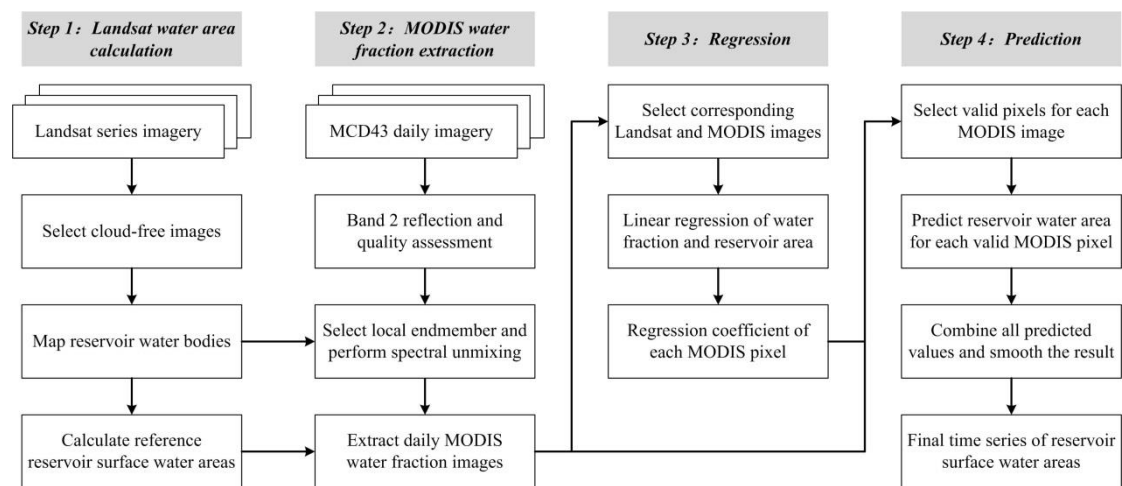

Fig. 3. Flowchart of the proposed method

3.1 Landsat water area calculation

In this step, reference reservoir surface water areas were calculated from cloud-free Landsat images. For a target reservoir, a region of interest (ROI) was defined by buffering the initial reservoir water extent in the Global Reservoir and Dam database (GRanD) (Lehner et al. 2011). A ROI image was clipped out from the original Landsat images, and the Modified Normalized Difference Water Index (MNDWI) (Xu 2006) was calculated as:

13

$$MNDWI = \frac{\rho_{GREEN} - \rho_{MIR}}{\rho_{GREEN} + \rho_{MIR}} \tag{1}$$

where ρ_{GREEN} is the green band reflectance of Landsat images (band 2 for TM and band 3 for OLI), and ρ_{MIR} is the middle infrared band reflectance of Landsat images (band 5 for TM and band 6 for OLI).

Water bodies were extracted from the MNDWI images using the OTSU algorithm (Li et al. 2013b), which can determine the optimal threshold value automatically and adaptively for each ROI image. From each extracted water map, the reservoir surface water area at the time of Landsat image acquisition was estimated by counting the number of pixels classed as water. Since the number of cloud-free Landsat images is limited, reservoir surface water area estimates from Landsat images are always not temporally dense. However, the finer spatial resolution of Landsat images helps to ensure that the surface water area estimates are more accurate than those derived from MODIS images.

3.2 MODIS water fraction extraction

In this step, daily water fraction images were extracted from original MODIS images by spectral unmixing. Here, the linear spectral mixture model was used. For a coarse spatial resolution pixel, the spectrum is calculated as a linear sum of each endmember weighted by its fractional cover (Settle and Drake 1993):

$$\rho'_{\lambda} = \sum_{i=1}^{N} f_i \times \rho_{i\lambda} + \varepsilon_{\lambda} \tag{2}$$

where ρ'_{λ} is the reflectance of a coarse resolution pixel at the spectral band λ, N is the number of endmembers, $\rho_{i\lambda}$ is the reflectance and f_i is the fractional cover of the ith endmember, and ε_{λ} is the residual term.

The linear spectral unmixing model was applied to the data acquired in MODIS band 2 and only two land cover classes, water and land, were considered. From equation (2), the water fraction f_{water} can then be estimated as:

$$f_{water} = \frac{\rho_{land} - \rho_M}{\rho_{land} - \rho_{water}} \tag{3}$$

where ρ_M is the reflectance of target MODIS pixel, ρ_{land} is the land reflectance, and ρ_{water} is the water reflectance.

Central to an accurate spectral unmixing analysis is the definition of the endmember spectra. Here, endmembers were computed locally in recognition of the potentially high degree of intra-class spectral variability. The unmixing analysis was then performed on all of the possible mixed pixels present in the ROI. To identify the possible mixed pixels, the minimal and maximal water extents were first estimated from Landsat images and all MODIS pixels were then separated to three categories: pure water pixels, pure land pixels and pixels with various fractions, according to their spatial relationships with the minimal and maximal water extents, as shown in Fig. 1. Pixels with various fractions may be mixed pixels or pure pixels with the water levels, and they are considered as possible mixed pixels. For each possible mixed MODIS pixel, the water and land reflectances were computed within a local spatial window centred on it. Here, the latter were estimated to be the median reflectances calculated across all relevant pure water and pure land pixels in the local window, which is set to be 15×15 in the MODIS image in this study.

3.3 Regression analysis

In this step, for each possible mixed MODIS pixel, a linear regression model between the

reservoir surface water area and the pixel water fraction was built as:

$$A^t = a_{ij} F_{ij}^t + b_{ij} \tag{4}$$

where A^t is the whole reservoir water area that is estimated from the Landsat image at time t, F_{ij}^t is the water fraction in the MODIS pixel *(i,j)* that is calculated from the MODIS band 2 image using the spectral unmixing model shown in Equation (3) at the same time t, and a_{ij} and b_{ij} are model parameters for the MODIS pixel *(i,j)*, which will not change over time and can be estimated by least square regression.

In practice, however, not all MODIS pixel water fractions could be used for regression. For a possible mixed pixel, when it is saturated (fully occupied by water or land), the water fraction value can not provide useful information about the reservoir surface water area. For example, water fractions in the pixel I should be 100% at both the maximal and instantaneous water levels (Fig. 1). Therefore, the water fraction values F_{ij}^t used for regression are limited in the range of [20%, 80%], aiming to remove those saturated pixels. The values of 20% and 80% are selected empirically to consider water fraction errors caused by spectral unmixing. Moreover, for a possible mixed pixel, if the difference between the largest and smallest values of water fractions is too small, the robustness of regression is hard to be ensured, consider the fraction errors caused by spectral unmixing. Therefore, the linear regression was not performed in the possible mixed MODIS pixels with the fraction value range less than a threshold, which is set to be 0.3 experimentally in this study.

For each MODIS pixel *(i,j)*, the correlation coefficient between the reservoir surface water area and the pixel water fraction, $R_{reg}(i, j)$, was also calculated from the same dataset used for regression. R_{reg} indicated the level of agreement between the pixel water fraction and the

reservoir surface water area. A higher R_{reg} value in one MODIS pixel means that the water fraction value of that pixel was more closely related to the whole reservoir surface water area, and hence would be more suitable for the prediction of water area than a pixel with a lower R_{reg} value. Thus, only the pixels with a large R_{reg} value was used in the generation of the time series of water areas. Here, the threshold value for use was $R_{reg} \geq 0.5$.

3.4 Predict time series of reservoir water areas

Using the regression model parameters a_{ij} and b_{ij}, the time series of reservoir water areas was predicted from daily MODIS water fraction images with equation (4). At time t, the MODIS pixels with water fractions in the range of [0.2, 0.8] were first determined. Then, among these MODIS pixels, the highest R_{reg} value, $R_{reg}^{\max}(t)$, was identified. Finally, the MODIS pixel *(i,j)* is further selected from those pixels with water fractions in the range of [0.2, 0.8] for water area prediction as:

$$R_{reg}(i, j) \in [\max[(R_{reg}^{\max}(t) - 0.2), 0.5], R_{reg}^{\max}(t)] \tag{5}$$

It should be noted that $R_{reg}(i, j)$ is constant in time but $R_{reg}^{\max}(t)$ may vary at different times, because the pixels with water fractions in the range of [0.2, 0.8] change with the water extent and cloud contamination. As a result, different pixels may be selected for different MODIS images. One reservoir surface water area can be predicted from each selected MODIS pixel, and by averaging predicted values of all selected pixels, the final reservoir water area at this day was obtained.

Once the time series of reservoir water areas is predicted from daily MODIS images, it is further smoothed with a low pass filter (averaging moving window), in order to smooth the effect of the noise in the original predicted time series. In this study, the size of the moving

average window was set to be 16 days, as the revisit time of MODIS is 16 days and the used

MCD43A4 Version 6 dataset is produced daily using 16 days of Terra and Aqua MODIS data,

by assigning the highest temporal weight to the day of interest (Tarpanelli et al. 2019).

3.5 Performance analysis

The accuracy of the predicted reservoir surface water areas was assessed with the water

levels acquired by satellite altimetry. The magnitude of the Pearson's coefficient correlation

between water area and water level (R_{pre}) was used to assess model performance (Khandelwal

et al. 2017).

4. Results

The proposed method was applied to the 21 selected reservoirs. For ease of discussion the

results for a single reservoir are presented first and discussed before considering the results

obtained over all reservoirs. .

4.1 The case study

The case study reservoir is Lake Sinakharin, Thailand with the identify number of 5161 in

the GRanD dataset. This reservoir is approximately 350 km^2 in area and is centered at 14.75°N

and 99.05°E. It has a dynamic region width about 0.94 km, and the correlation coefficient

between water levels acquired by satellite altimetry and water areas generated from the MODIS

images with the pixel based analysis method proposed by Khandelwal et al. (2017) is 0.47.
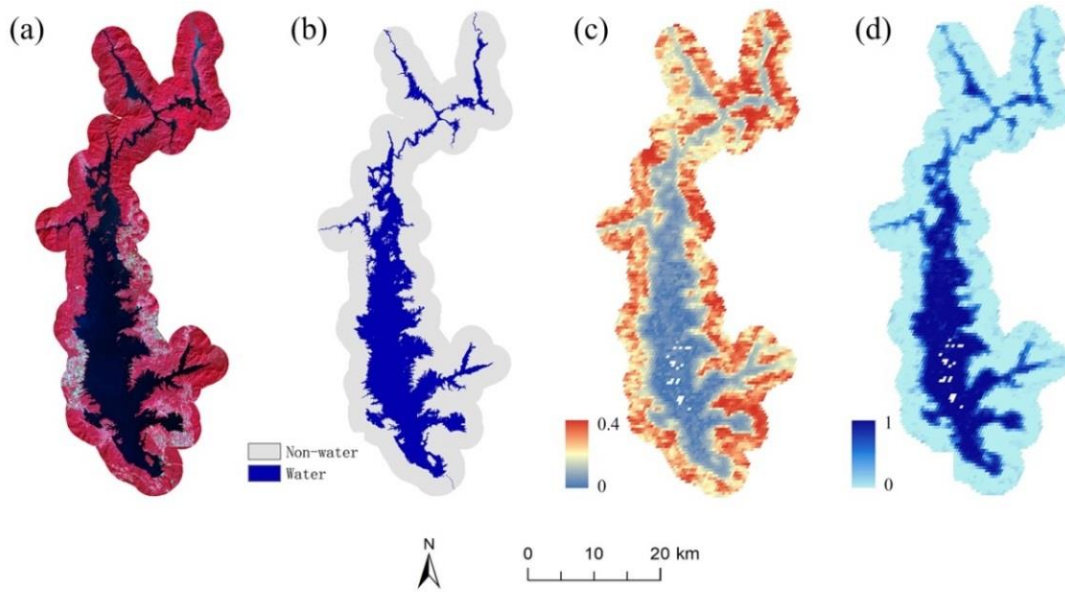
Fig. 4. Example images acquired at November 3rd, 2018, in the Lake Sinakharin, Thailand. (a) False color Landsat OLI image (RGB: Bands 5, 4 and 3) with a spatial resolution of 30 m; (b) Water body extracted from the Landsat OLI image; (c) The MODIS band 2 image with a spatial resolution of 500 m; (d) The water fraction image estimated from MODIS. The water boundary is well represented by Landsat images in (a) and (b). Blocky pixels are clear and the water boundary cannot be accurately mapped from the MODIS image in (c) and (d).

The reservoir can be fully covered by one Landsat scene, and there are 45 cloud-free Landsat scenes available during the period of 2001 to 2018. For each Landsat scene, the ROI image was clipped out (Fig. 4(a)), the water body was extracted (Fig. 4(b)) and used to calculate the reservoir water area on the data of Landsat image acquisition. As a result, there were 45 reference reservoir surface water areas available. Meanwhile, the spectral unmixing analysis was applied on the MODIS band 2 image acquired on the same day as the Landsat scene (Fig. 4(c)), to estimate the water fraction image (Fig. 4(d)). Moreover, the 45 corresponding MODIS water fraction images have also been produced. This dataset was used in a series of regression analyses.
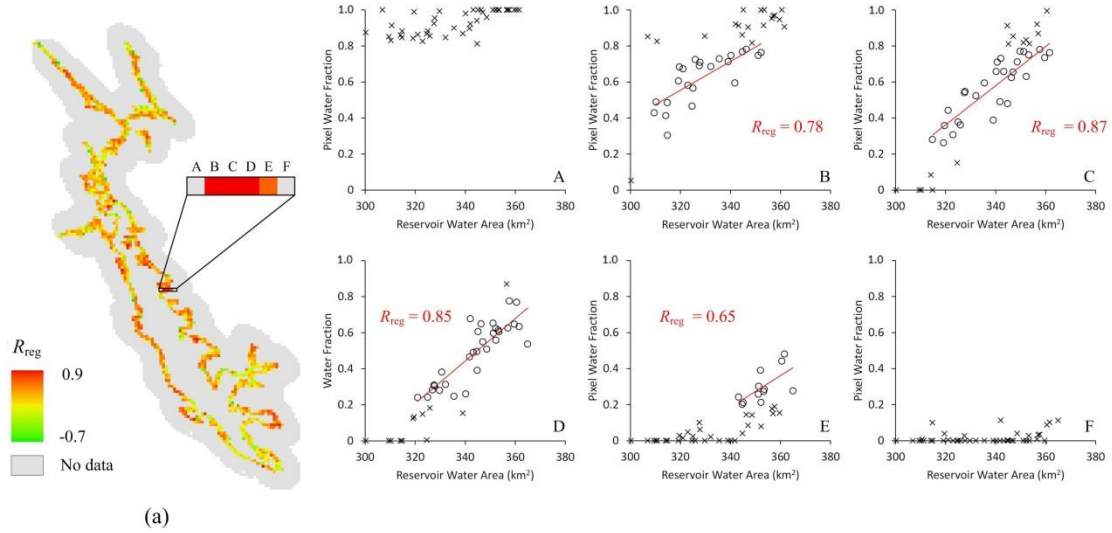
Fig. 5. Regression results in the Lake Sinakharin, Thailand. (a) R_{reg} values between water fractions and reservoir surface water areas for all MODIS pixels. (b) Linear regression results of six MODIS pixels shown in (a). Water fraction values outside the range of [0.2, 0.8] are marked by crosses and are not used for regression. Water fraction values within the range of [0.2, 0.8] are marked by circles and used for regression.

For each MODIS pixel, a linear regression was performed with its corresponding water fractions and reservoir water areas. Noticed that there were 45 reservoir water areas available, but the corresponding water fractions may be void due to the data quality of MODIS. In this situation, the number of pairs of reservoir water areas and water fractions used for the regression is decreased. Fig. 5(a) shows R_{reg} values between water fractions and reservoir water areas and Fig. 5(b) shows linear regression results of six adjacent MODIS pixels from the inside to the outside of the reservoir. It is noticed that the pixel A located inside the reservoir is always representing an area full of water, while the pixel F located outside of the reservoir is always representing an area full of land. In these two situations, no water fraction values can be used for regression, and both MODIS pixels have no R_{reg} values. The MODIS pixels located along

20

the reservoir boundary often have relative high R_{reg} values, such as the pixel B, C, D and E. These pixels are suitable for the prediction of the reservoir surface water area if they have water fraction values. In Fig. 5(a), it is also noticed that a small part of pixels have low or even negative R_{reg} values. This is mainly caused by the errors of pixel water fraction produced by the spectral unmixing analysis. In practice, however, these pixels will not have impacts on the result, because the MODIS pixels with R_{reg} values less than 0.5 are not used for prediction in the proposed method.

Fig. 6 shows the reservoir surface water area prediction process in two different days for comparison. Fig. 6(a) and (d) show the MODIS band 2 images acquired on Feb. 28th, 2000 and May 29th, 2003, respectively. Both images have no data in some areas caused by cloud contamination and this problem is more serious in the latter image. Fig. 6(b) and (e) show their corresponding water fraction images estimated by spectral unmixing. By overlaying the water fraction image with R_{reg} values in Fig. 5(a), the MODIS pixels used for prediction are selected. Because the water fraction images are different in these two days, these selected MODIS pixels are also different (Fig. 6(c) and (f)). With these selected MODIS pixels, the reservoir surface water area at the time of satellite observation can then be predicted from their water fraction values and associated regressed linear functions.
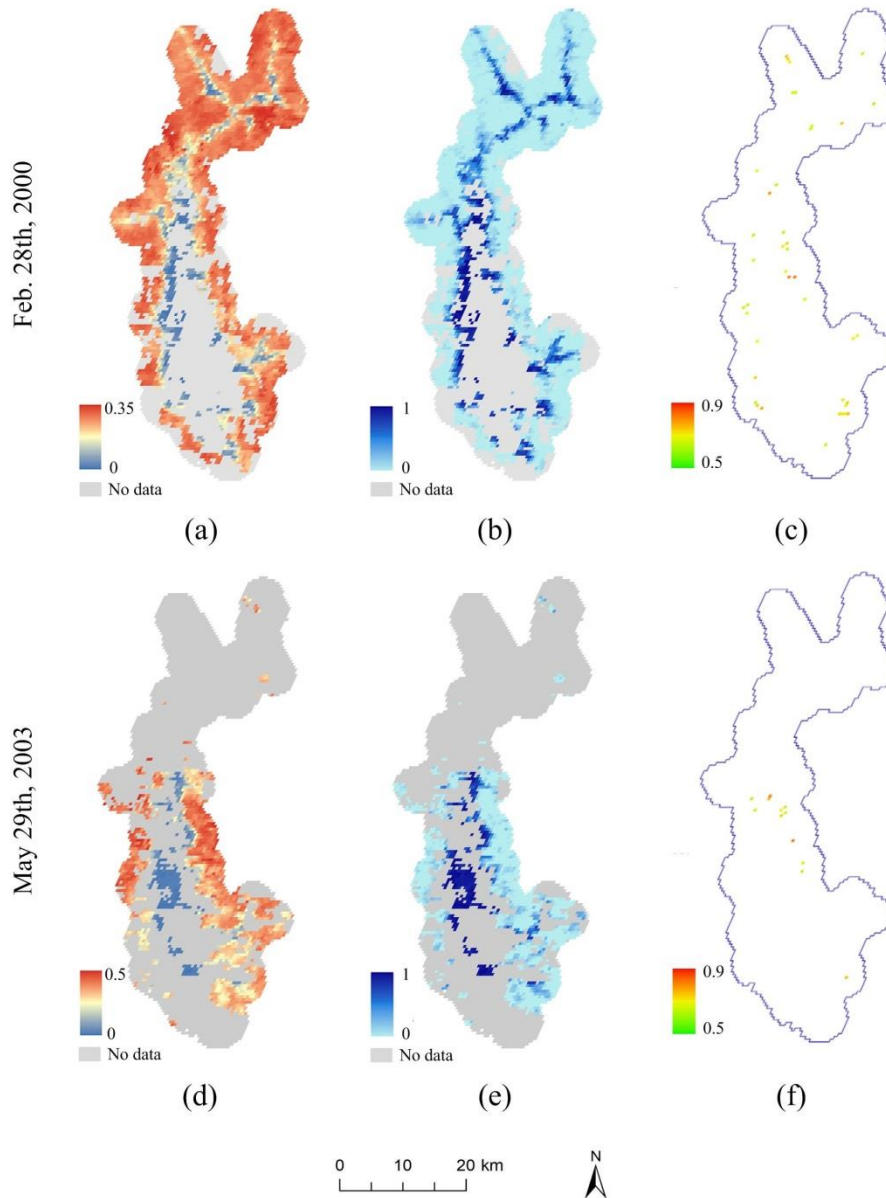
Fig. 6. Examples of valid MODIS pixels selection in the prediction process. (a) and (d) are MODIS band 2 images acquired on Feb. 28th, 2000 and May 29th, 2003, respectively. (b) and (e) are corresponding water fraction images of (a) and (d), respectively. (c) and (f) are R_{reg} values of selected MODIS pixels for prediction of (a) and (d), respectively. Both MODIS images have no data in some areas caused by cloud contamination, and this problem in (d) is more serious than that in (a), especially in the northern area.
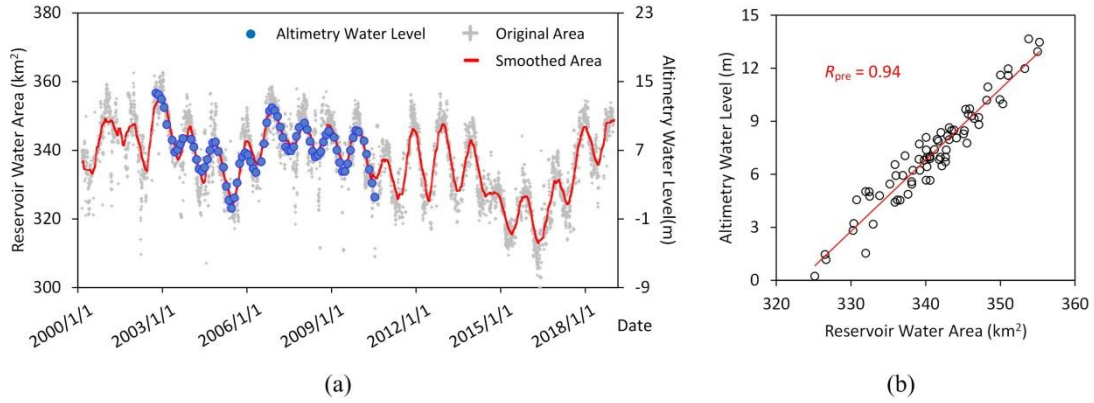
Fig. 7. Results of Lake Sinakharin, Thailand. (a) Original and smoothed time series of reservoir water areas (km²) from 2000 to 2018 marked by grey crosses and red lines, with water levels (m) monitored by satellite altimetry marked by blue circles. (b) Comparison of smoothed surface area (km²) with altimetry water levels (m).

Fig. 7(a) shows the resultant time series of reservoir surface water areas predicted from the MODIS images. The original time series marked by grey crosses includes a large number of unreasonable fluctuations, which may be caused by errors included in water fraction values and regressed linear equations of the used MODIS pixels. The noise in the original time series were well filtered through the moving average window filter used in the proposed method, and the resultant smoothed time series of reservoir surface water areas shows a relatively high degree of agreement with the reservoir water levels monitored by satellite altimetry. Fig. 7(b) shows the scatter plot between smoothed time series of reservoir surface water areas and altimetry water levels. R_{pre} reaches 0.94 that is much higher than the value (0.47) reported by Khandelwal et al. (2017), illustrating the effectiveness of the proposed method for this reservoir.

4.2 Results for all reservoirs

Table 1. Validation of reservoir surface water areas predicted by the proposed method using correlation coefficients with altimetry water levels (R_{pre}).

No.	Reservoir	GRanD ID	Location	Area (km²)	Dynamic region width (m)	Landsat images number	R_{pre} Khandelwal et al. (2017)	R_{pre} The proposed method
1	Flathead	316	47.90°N, 114.11°W	496	504	43	-0.02	0.81
2	Livingston	1287	30.71°N, 95.13°W	224	1070	69	0.25	0.53
3	Dale Hollow	1762	36.61°N, 85.31°W	93	2363	48	-0.23	0.50
4	Hartwell	1851	34.41°N, 82.85°W	200	2649	81	0.33	0.90
5	Murray	1866	34.06°N, 81.31°W	170	1415	74	0.23	0.85
6	Marion	1879	33.45°N, 80.33°W	225	814	95	0.33	0.82
7	St.Jean	2021	48.60°N, 72.05°W	1072	633	19	0.21	0.56
8	Bariri	2397	21.47°S, 49.49°W	525	912	97	0.4	0.83
9	Barra Bonita	2414	23.29°S, 48.98°W	405	1830	15	0.21	0.76
10	Krasnooskol	4370	49.30°N, 37.60°E	85	871	41	0.05	0.65
11	Sinakharin	5161	14.75°N, 99.05°E	350	941	45	0.47	0.94
12	Itaipu	2432	24.89°S, 54.42°W	1270	969	64	0.32	0.44
13	Hongze	5295	33.29°N, 118.64°E	1473	1333	46	0.27	0.45
14	Volgogradskoye	4372	50.36°N, 45.87°E	2650	630	18	0.15	0.35
15	Kakhovskoye	4376	47.53°N, 34.46°E	2130	613	22	-0.36	0.30
16	Nipigon	1402	49.82°N, 88.46°W	4520	560	14	-0.1	0.01
17	Winnebago	1493	44.02°N, 88.42°W	648	540	30	-0.03	-0.20
18	Kasumiga-ura	6453	36.04°N, 140.40°E	168	577	43	-0.16	-0.25
19	Ontario	1485	43.68°N, 77.86°W	19400	621	1	-0.38	-
20	Kremenshugskoye	4371	49.27°N, 32.68°E	1880	1118	1	0.48	-
21	Victoria	4492	0.99°S, 32.87°E	69400	559	0	0.27	-

Table 1 shows the resultant correlation coefficients (R_{pre}) between predicted time series of surface water areas and altimetry water levels in all reservoirs, which are distributed in different locations all over the world and have different climate, hydrological and geomorphological features. R_{pre} values predicted from the MODIS images based on the pixel based analysis method reported by Khandelwal et al. (2017) are all less than 0.5. With the

proposed method for surface water area estimation, for most of these study reservoirs, R_{pre}

values are increased from very low values to much higher values.

For just over half of the reservoirs (No. 1 to No. 11 in Table 1) R_{pre} values are greater

than 0.5. Six reservoirs have R_{pre} values greater than 0.8, and the largest R_{pre} value reaches

0.94. The mean R_{pre} value of these 11 reservoirs is 0.74, and is much larger than that obtained

from the pixel based analysis method reported by Khandelwal et al. (2017), which is only 0.20.

There are other four reservoirs (No. 12 to No. 15) with R_{pre} values larger than 0.3 but less

than 0.5. Although R_{pre} values are relatively low they are still larger than those obtained from

the application of the pixel based method.

The proposed method yielded poor results for three reservoirs (No. 16 to No. 18). The

Nipigon (No. 16) and Kakhovskoye (No. 17) reservoirs are located in the high latitudes. Both

reservoirs are often covered by ice, and ice is spectrally very different to both land and water.

The poor performance of the proposed method in the Kasumiga-ura (No. 18) reservoir is

perhaps caused by the uncertainty of the reference reservoir surface water areas calculated from

Landsat images, which was also found to have a very low correlation coefficient value with the

altimetry water levels.

For the remaining three reservoirs (No. 19 to No. 21), R_{pre} values were not calculated.

The main reason for this situation is that cloud-free Landsat images covering the whole

reservoir were difficult to be acquire. As a result there was insufficient reference reservoir

surface area data for regression analysis. Consequently, a time series of reservoir surface water

area could not be predicted from the fraction images for these reservoirs. Future studies could

perhaps use radar imagery such as from Sentinel 1 rather than Landsat to form the reference data on surface water area required.

5. Discussion

In order to monitor reservoir surface water areas at a fine temporal resolution, the coarse imagery with a high re-visit frequency should be used in practice. However, there are two key problems need to be addressed. First, the reservoir may not be entirely visible because of the cloud contamination, and second the coarse image pixel size makes the mixed pixel problem serious, limiting the accuracy of standard pixel based methods.

The experimental results presented above showed that estimating water fractional values at the sub-pixel scale is useful to address the mixed pixel problem encountered with coarse spatial resolution images. The change in water fractions for MODIS pixels located along the reservoir boundary is often closely related to the reservoir water area variation, and their relationship makes it possible to directly estimate the whole reservoir water area from, potentially, an individual cloud-free MODIS pixel. Therefore, using sub-pixel information is promising means to reduce the negative effects caused by the coarse spatial resolution and the cloud contamination simultaneously. The proposed method predicted the time series of reservoir surface water areas with a relative high accuracy, however, some issues about its performance should be considered in future research and its practical application.
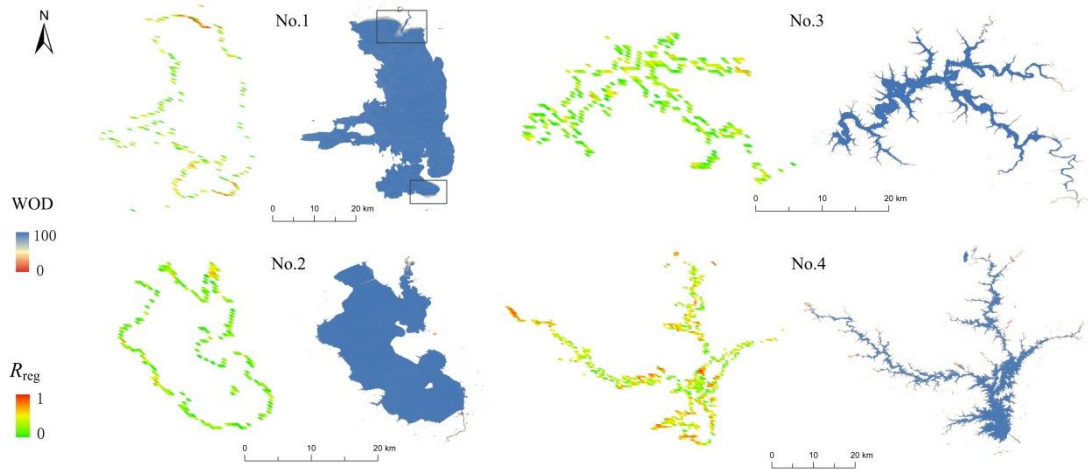
Fig. 8. Regression results (R_{reg}) and water occurrence datasets (WOD) images of the first 4 reservoirs/lakes in Table 1. The pixel value in WOD represents the frequency (in percentage) that the pixel was covered by water. No. 1 is Flathead Lake (R_{pre} =0.81), No. 2 is Livingston Lake (R_{pre} =0.53), No. 3 is Dale Hollow reservoir (R_{pre} =0.50), and No. 4 is Hartwell reservoir (R_{pre} =0.90).

5.1 The usability of MODIS pixels

Different from general land cover classes, the spatial distribution of water bodies has a special feature, that is, it is basically controlled by the reservoir bathymetry and associated with the water level, as shown in Fig. 1. This feature provides a great chance to improve the usability of remote sensing images in reservoir water surface monitoring. In the proposed method, the whole reservoir surface water area is directly linked with the sub-pixel water coverage information in those MODIS pixels located near the reservoir boundary. Therefore, ideally, only one MODIS pixel is enough to predict the whole surface water area, once the water coverage in this pixel can well represent the feature of reservoir water area variation.

Whether a MODIS pixel can be used for reservoir area prediction mainly depends on the value of R_{reg}. Fig. 8 shows the regression results (R_{reg}) and water occurrence dataset (WOD) images of the first 4 reservoirs/lakes in Table 1. Here, the WOD value represents an estimate

27

of the inundation frequency (in percentage) that the pixel was covered by water. It was generated by stacking all of the monthly water coverage images produced from a 32-year Landsat image collection (Pekel et al. 2016), and provides a detailed spatial distribution of the dynamic region of each reservoir. It should be noted that, although a single value of dynamic region width coming from Khandelwal et al. (2017) is provided for each reservoir in Table 1, this single value cannot exactly represent the overall dynamic range, because the dynamic ranges at different parts of the reservoir are different. In Fig. 8, it is noticed that the R_{reg} value is affected by the dynamic region width to some extent. For example, in the Flathead Lake (No. 1), the dynamic region widths within the top and bottom rectangles are much larger than the widths in other locations, and the corresponding R_{reg} values are also higher than other values. Similar patterns are noticed in other reservoirs. In general, the terrain boundary in the area with a small dynamic region width is often sharp. Water fraction variations in these MODIS pixel are then too small to be accurately monitored, leading to a low R_{reg} value. Conversely, the terrain boundary is gradual when the dynamic region width is large, and the regression often has a high R_{reg} value.

The accuracy of predicted reservoir water areas is largely determined by the regression result. It is assumed that using a MODIS pixel with a higher R_{reg} value can predict the whole reservoir surface water area more accurately than using a pixel with a lower R_{reg} value. In Fig. 8, there are a large number of MODIS pixels with $R_{reg} \geq 0.8$ in the No. 1 and No. 4 reservoirs, and both predicted results have high R_{pre} values (0.81 and 0.90). In the No. 2 and No. 3 reservoirs, however, there are few MODIS pixels with $R_{reg} \geq 0.8$ and the predicted

results are much worse. The result demonstrates the importance of the R_{reg} value in regression to final reservoir water area prediction.

In the prediction process, only a part of MODIS pixels were selected based on the value of R_{reg}. There are several possible strategies to select prediction MODIS pixels, for example, selecting all MODIS pixels with $R_{reg} \geq 0.5$ or selecting the single MODIS pixel with the highest R_{reg} value. On the one hand, the highest R_{reg} value in many reservoirs could reach about 0.8 or 0.9. Considering using a MODIS pixel with $R_{reg} \geq 0.8$ may predict the area more accurately than using a pixel with the R_{reg} value near 0.5, selecting all MODIS pixels with $R_{reg} \geq 0.5$ will decrease the accuracy of the prediction. On the other hand, there are also some problems when only the MODIS pixel with the highest R_{reg} value is selected. There often exist some MODIS pixels with R_{reg} values only a little smaller than the highest one, and the prediction result is unstable when only a single MODIS pixel is used due to the uncertainty of spectral unmixing. In this study, therefore, some MODIS pixels with high R_{reg} values were selected together according to Equation (5) and the final reservoir water area was estimated by averaging the predicted values of these selected MODIS pixels. This strategy can overcome the shortcomings of the other two strategies to some extent. There are, of course, some possible improvements, such as using a better rule to select MODIS pixels or using a weighted average to estimate the final area by taking account of the R_{reg} value of each used MODIS pixel.

5.2 Error sources and Uncertainty analysis

In the proposed method, the reservoir surface water area is estimated from the MODIS pixel water fraction using the linear regression equation (4). The accuracy of the predicted reservoir surface water area depends greatly on the accuracy of the input pixel water fraction

value. Errors included in the MODIS water fraction images will decrease the result accuracy.

In this study, for simplicity, the spectral unmixing analysis had been applied to imagery

acquired in only MODIS band 2 and only two land cover classes, water and land, were

considered. As a result, the estimated water fraction may have large uncertainty due to the

spectral variations of both land cover classes, especially for the class of land that may includes

vegetation, bare land, and other objects. It is also noticed that shadows are common in some

reservoirs, and they have similar spectral reflectance values as water bodies and then will bring

uncertainty to the estimated water fraction image.

For both regression and prediction processes, those saturated MODIS pixels should not be

used. Ideally, the pixel with the water fraction value of zero should be regarded as a full land

pixel, while the pixel with the water fraction value of one should be regarded as a full water

pixel. However, considering water fraction errors caused by spectral unmixing, the values of

zero and one are unsuitable in practice. For example, in Fig. 5, the pixel A was always full of

water, but the estimated water fraction values always included errors caused by spectral

unmixing and then were larger than zero. Therefore, a suitable range should be selected to

remove those saturated pixels. If the range is too small, the water fraction values used for

regression will be too few; if the range is too large, many incorrect water fraction values will

be used for regression. After experiment, the range of [0.2, 0.8] was selected in this study, and

it was found that the values of R_{pre} with this range were higher than those with the ranges of

[0.1, 0.9] and [0.3, 0.7]. It should be noted that, however, although the range [0.2, 0.8] is

acceptable in most cases, it is not perfect and the best range should be different for various

reservoirs.

The linear function used for reservoir water area prediction is another crucial issue that impacts on the accuracy of surface water area estimation. The linear regression of the reference water areas and the corresponding pixel water fraction values will, however, be impacted by errors in the two data sets and hence there is some uncertainty in the predictions from the regression model. In addition, when the reservoir surface water area is larger than the maximum area or is less than the minimum area calculated from cloud-free Landsat images, it is really predicted by extrapolation with the regressed linear equations, and this then may unavoidably includes errors.

5.3 Future works and applications

The effectiveness of the proposed method has been illustrated with experimental results, however, there are means to further improve the performance in the future. First, the linear spectral unmixing algorithm used in this study should be improved, for example, by using more spectral bands of MODIS images and other nonlinear spectral unmixing models, or using more ancillary data, such as the water occurrence dataset, in the spectral unmixing model. Second, the quality of reference reservoir surface water areas could be improved. More powerful water mapping algorithms or post-processing methods can be used to calculate the water areas more accurately. Other satellite sensors, such as those on Sentinel-1 and Sentinel-2, could be used to provide more remotely sensed images to increase the number of reference water areas available. Third, using better temporal filter algorithms and fusing the water areas predicted from MODIS images and the reference water areas calculated from Landsat images are useful to increase the accuracy and robustness of the final water area time series.

The proposed method has more possible applications in the future. The proposed method was applied on the MODIS images in this study, however, it can be easily extended to other remotely sensed images, such as the new Sentinel-3 Ocean and Land Colour Instrument (OLCI) images. The only necessary modification is selecting suitable spectral bands for those images. The proposed method can also be applied on the Landsat images, given the spatial resolution of Landsat images is still too coarse to monitor the surface water area variations for many reservoirs globally. Although the proposed method only estimates the reservoir surface water area time series in this study, the result can be further analyzed to provide additional useful information. For example, the change of reservoir water volumes could be predicted by combining the surface water area with the water levels monitored by satellite altimetry.

6. Conclusion

Reservoir surface water area is often monitored by remotely sensing. MODIS is an attractive data source in the monitoring of reservoir surface water area variation, as it has a daily re-visit frequency globally. In practice, however, the usability of the MODIS images is often constrained by their coarse spatial resolution problem and the effects of cloud contamination. Presently, there is no established approach to solve both problems simultaneously limiting the ability to monitor reservoirs in an accurate and timely manner at regional to global scales. This study proposed an approach to monitor reservoir surface water area variations from the MODIS images through the use of sub-pixel scale information. The approach used water fractions extracted from the MODIS images and reference reservoir surface water areas calculated from cloud-free Landsat images to construct linear regression functions for each MODIS pixel. A time series of reservoir surface water areas can then be

32

predicted from the extracted daily MODIS water fraction images using the constructed linear regression functions.

The performance of the proposed approach was assessed with a set of reservoirs for which standard pixel-based approaches have been found to be inaccurate. The results show that the proposed method can greatly reduce the negative impacts caused by the coarse spatial resolution problem and the cloud contamination problem of the MODIS images. Compared with the conventional pixel based analysis approach, the proposed method can substantially increase the accuracy of reservoir surface water area prediction. The experimental results illustrate the value of sub-pixel information in reservoir monitoring from coarse spatial resolution remotely sensed imagery. The proposed approach is valuable to improve the usability and effectiveness of existing remote sensing systems in monitoring reservoir surface water area variations globally, and can be easily extended to other types of remotely sensed images and to additional practical applications in the future.

Acknowledgment

References

Alsdorf, D.E., Rodriguez, E., & Lettenmaier, D.P., 2007. Measuring surface water from space. *Reviews of Geophysics 45*:RG2002.

Arvor, D., Daher, F.R.G., Briand, D., Dufour, S., Rollet, A.-J., Simões, M., et al., 2018. Monitoring thirty years of small water reservoirs proliferation in the southern Brazilian Amazon with Landsat time series. *ISPRS Journal of Photogrammetry and Remote Sensing 145*:225-237.

Avisse, N., Tilmant, A., Muller, M.F., & Zhang, H., 2017. Monitoring small reservoirs' storage with satellite remote sensing in inaccessible areas. *Hydrology and Earth System Sciences 21*:6445-6459.

Birkett, C.M., 1995. The contribution of TOPEX/POSEIDON to the global monitoring of climatically sensitive lakes. *Journal of Geophysical Research-Oceans 100*:25179-25204.

Birkett, C.M., & Beckley, B., 2010. Investigating the Performance of the Jason-2/OSTM Radar Altimeter over Lakes and Reservoirs. *Marine Geodesy 33*:204-238.

Busker, T., de Roo, A., Gelati, E., Schwatke, C., Adamovic, M., Bisselink, B., et al., 2019. A global lake and reservoir volume analysis using a surface water dataset and satellite altimetry. *Hydrology and Earth System Sciences 23*:669-690.

Chen, L., Michishita, R., & Xu, B., 2014. Abrupt spatiotemporal land and water changes and their potential drivers in Poyang Lake, 2000–2012. *ISPRS Journal of Photogrammetry and Remote Sensing 98*:85-93.

Cretaux, J.F., Abarca-del-Rio, R., Berge-Nguyen, M., Arsen, A., Drolon, V., Clos, G., et al., 2016. Lake Volume Monitoring from Space. *Surveys in Geophysics 37*:269-305.

Doernhoefer, K., & Oppelt, N., 2016. Remote sensing for lake research and monitoring - Recent advances. *Ecological Indicators 64*:105-122.

Downing, J.A., Prairie, Y.T., Cole, J.J., Duarte, C.M., Tranvik, L.J., Striegl, R.G., et al., 2006. The global abundance and size distribution of lakes, ponds, and impoundments. *Limnology and Oceanography 51*:2388-2397.

Duan, Z., & Bastiaanssen, W.G.M., 2013. Estimating water volume variations in lakes and reservoirs from four operational satellite altimetry databases and satellite imagery data. *Remote Sensing of Environment 134*:403-416.

Feyisa, G.L., Meilby, H., Fensholt, R., & Proud, S.R., 2014. Automated Water Extraction Index: A new technique for surface water mapping using Landsat imagery. *Remote Sensing of Environment 140*:23-35.

Foody, G.M., & Cox, D.P., 1994. Sub-pixel land cover composition estimation using a linear mixture model and fuzzy membership functions. *International Journal of Remote Sensing 15*:619-631.

Frazier, P.S., & Page, K.J., 2000. Water body detection and delineation with Landsat TM data. *Photogramm. Eng. Remote Sens. 66*:1461-1467.

Gao, H., 2015. Satellite remote sensing of large lakes and reservoirs: from elevation and area to storage. *Wiley Interdisciplinary Reviews-Water 2*:147-157.

Gao, H., Birkett, C., & Lettenmaier, D.P., 2012. Global monitoring of large reservoir storage from satellite remote sensing. *Water Resources Research 48*:W09504.

Gorelick, N., Hancher, M., Dixon, M., Ilyushchenko, S., Thau, D., & Moore, R., 2017. Google Earth Engine: Planetary-scale geospatial analysis for everyone. *Remote Sensing of Environment 202*:18-27.

Huang, C., Chen, Y., Zhang, S., & Wu, J., 2018. Detecting, Extracting, and Monitoring Surface Water From Space Using Optical Sensors: A Review. *Reviews of Geophysics 56*:333-360.

Keshava, N., & Mustard, J.F., 2002. Spectral unmixing. *IEEE Signal Process. Mag. 19*:44-57.

Khandelwal, A., Karpatne, A., Marlier, M.E., Kim, J., Lettenmaier, D.P., & Kumar, V., 2017. An approach for global monitoring of surface water extent variations in reservoirs using MODIS data. *Remote Sensing of Environment 202*:113-128.

Klein, I., Gessner, U., Dietz, A.J., & Kuenzer, C., 2017. Global WaterPack - A 250 m resolution dataset revealing the daily dynamics of global inland water bodies. *Remote Sensing of Environment 198*:345-362.

Lehner, B., Liermann, C.R., Revenga, C., Voeroesmarty, C., Fekete, B., Crouzet, P., et al., 2011. High-resolution mapping of the world's reservoirs and dams for sustainable river-flow management. *Frontiers in Ecology and the Environment 9*:494-502.

Li, L., Skidmore, A., Vrieling, A., & Wang, T., 2019a. A new dense 18-year time series of surface water fraction estimates from MODIS for the Mediterranean region. *Hydrology and Earth System Sciences 23*:3037-3056.

Li, S., Sun, D., Goldberg, M., & Stefanidis, A., 2013a. Derivation of 30-m-resolution water maps from TERRA/MODIS and SRTM. *Remote Sensing of Environment 134*:417-430.

Li, W., Du, Z., Ling, F., Zhou, D., Wang, H., Gui, Y., et al., 2013b. A comparison of land surface water mapping using the normalized difference water index from TM, ETM+ and ALI. *Remote Sensing 5*:5530-

5549.

Li, W., Zhang, X., Ling, F., & Zheng, D., 2016. Locally adaptive super-resolution waterline mapping with MODIS imagery. *Remote sensing letters 7*:1121-1130.

Li, X., Wang, L., Cheng, Q., Wu, P., Gan, W., & Fang, L., 2019b. Cloud removal in remote sensing images using nonnegative matrix factorization and error correction. *ISPRS Journal of Photogrammetry and Remote Sensing 148*:103-113.

Ling, F., Boyd, D., Ge, Y., Foody, G.M., Li, X., Wang, L., et al., 2019. Measuring River Wetted Width From Remotely Sensed Imagery at the Subpixel Scale With a Deep Convolutional Neural Network. *Water Resources Research 55*:5631-5649.

Ma, B., Wu, L., Zhang, X., Li, X., Liu, Y., & Wang, S., 2014. Locally adaptive unmixing method for lake-water area extraction based on MODIS 250 m bands. *International Journal of Applied Earth Observation and Geoinformation 33*:109-118.

Ma, Y., Xu, N., Sun, J., Wang, X.H., Yang, F., & Li, S., 2019. Estimating water levels and volumes of lakes dated back to the 1980s using Landsat imagery and photon-counting lidar datasets. *Remote Sensing of Environment 232*:111287.

McFeeters, S.K., 1996. The use of the normalized difference water index (NDWI) in the delineation of open water features. *International Journal of Remote Sensing 17*:1425-1432.

Muad, A.M., & Foody, G.M., 2012. Super-resolution mapping of lakes from imagery with a coarse spatial and fine temporal resolution. *International Journal of Applied Earth Observation and Geoinformation 15*:79-91.

Park, E., Lewis, Q.W., & Sanwlani, N., 2019. Large lake gauging using fractional imagery. *Journal of Environmental Management 231*:687-693.

Pekel, J.-F., Cottam, A., Gorelick, N., & Belward, A.S., 2016. High-resolution mapping of global surface water and its long-term changes. *Nature 540*:418-422.

Schwatke, C., Dettmering, D., Bosch, W., & Seitz, F., 2015. DAHITI - an innovative approach for estimating water level time series over inland waters using multi-mission satellite altimetry. *Hydrology and Earth System Sciences 19*:4345-4364.

Seaton, D., Dube, T., & Mazvimavi, D., 2020. Use of multi-temporal satellite data for monitoring pool surface areas occurring in non-perennial rivers in semi-arid environments of the Western Cape, South

Africa. *ISPRS Journal of Photogrammetry and Remote Sensing 167*:375-384.

Settle, J.J., & Drake, N.A., 1993. Linear mixing and the estimation of ground cover proportions. *International Journal of Remote Sensing 14*:1159-1177.

Sheng, Y., Song, C., Wang, J., Lyons, E.A., Knox, B.R., Cox, J.S., et al., 2016. Representative lake water extent mapping at continental scales using multi-temporal Landsat-8 imagery. *Remote Sensing of Environment 185*:129-141.

Tarpanelli, A., Amarnath, G., Brocca, L., Massari, C., & Moramarco, T., 2017. Discharge estimation and forecasting by MODIS and altimetry data in Niger-Benue River. *Remote Sensing of Environment 195*:96-106.

Tarpanelli, A., Brocca, L., Lacava, T., Melone, F., Moramarco, T., Faruolo, M., et al., 2013. Toward the estimation of river discharge variations using MODIS data in ungauged basins. *Remote Sensing of Environment 136*:47-55.

Tarpanelli, A., Santi, E., Tourian, M.J., Filippucci, P., Amarnath, G., & Brocca, L., 2019. Daily River Discharge Estimates by Merging Satellite Optical Sensors and Radar Altimetry Through Artificial Neural Network. *IEEE Transactions on Geoscience and Remote Sensing 57*:329-341.

Tong, X., Pan, H., Xie, H., Xu, X., Li, F., Chen, L., et al., 2016. Estimating water volume variations in Lake Victoria over the past 22 years using multi-mission altimetry and remotely sensed images. *Remote Sensing of Environment 187*:400-413.

Tulbure, M.G., & Broich, M., 2013. Spatiotemporal dynamic of surface water bodies using Landsat time-series data from 1999 to 2011. *ISPRS Journal of Photogrammetry and Remote Sensing 79*:44-52.

Van Dijk, A.I.J.M., Brakenridge, G.R., Kettner, A.J., Beck, H.E., De Groeve, T., & Schellekens, J., 2016. River gauging at global scale using optical and passive microwave remote sensing. *Water Resources Research 52*:6404-6418.

Verpoorter, C., Kutser, T., Seekell, D.A., & Tranvik, L.J., 2014. A global inventory of lakes based on high-resolution satellite imagery. *Geophysical Research Letters 41*:6396-6402.

Wang, Z., Schaaf, C.B., Sun, Q., Shuai, Y., & Roman, M.O., 2018. Capturing rapid land surface dynamics with Collection V006 MODIS BRDF/NBAR/Albedo (MCD43) products. *Remote Sensing of Environment 207*:50-64.

Wayand, N.E., Marsh, C.B., Shea, J.M., & Pomeroy, J.W., 2018. Globally scalable alpine snow metrics.

Remote Sensing of Environment 213:61-72.

Xu, H., 2006. Modification of normalised difference water index (NDWI) to enhance open water features in remotely sensed imagery. *International Journal of Remote Sensing 27*:3025-3033.

Yao, F., Wang, J., Wang, C., & Crétaux, J.-F., 2019. Constructing long-term high-frequency time series of global lake and reservoir areas using Landsat imagery. *Remote Sensing of Environment 232*:111210.

Zhang, G., Xie, H., Kang, S., Yi, D., & Ackley, S.F., 2011. Monitoring lake level changes on the Tibetan Plateau using ICESat altimetry data (2003-2009). *Remote Sensing of Environment 115*:1733-1742.

Zhang, H., Gorelick, S.M., Zimba, P.V., & Zhang, X., 2017. A remote sensing method for estimating regional reservoir area and evaporative loss. *Journal of Hydrology 555*:213-227.

Zhang, S., Gao, H., & Naz, B.S., 2014. Monitoring reservoir storage in South Asia from multisatellite remote sensing. *Water Resources Research 50*:8927-8943.

Zhao, G., & Gao, H., 2018. Automatic Correction of Contaminated Images for Assessment of Reservoir Surface Area Dynamics. *Geophysical Research Letters 45*:6092-6099.

Zhou, T., Nijssen, B., Gao, H., & Lettenmaier, D.P., 2016. The Contribution of Reservoirs to Global Land Surface Water Storage Variations. *Journal of Hydrometeorology 17*:309-325.